DOI: 10.1002/ejic.201100093

Spectroscopic, Electrochemical, and DFT Studies of Oxo-Centered Triruthenium Cluster Complexes with a Bis(tridentate) Triazine Ligand

Feng-Rong Dai,[a] Yu-Hui Wu,[a] Li-Yi Zhang,[a] Bin Li,[a] Lin-Xi Shi,[a] and Zhong-Ning Chen*[a]

Keywords: Ruthenium / Cluster compounds / N ligands / Redox chemistry / Density functional calculations

Oxo-centered triruthenium–acetate complexes with a tridentate or bis(tridentate) triazine ligand have been prepared by the reaction of $[Ru_3O(OAc)_6(py)_2(CH_3OH)]^+$ ($[\mathbf{1}]^+$) with a triazine ligand [3-(2-pyridyl)-1,2,4-triazine (pytz), 3-(2-pyrimidinyl)-1,2,4-triazine (pmtz), or 5,5′,6,6′-tetramethyl-3,3′-bi-1,2,4-triazine (bdmt)]. The dimeric complex $[\{Ru_3O(OAc)_5(py)_2\}_2(\mu_4\text{-pmtz})]^{2+}$ ($[\mathbf{5}]^{2+}$), an intercluster mixed-valence complex ($[Ru_3^{III,III,II}\text{-pmtz-}Ru_3^{III,III,III}]^{2+}$) containing an asymmetric bis(tridentate) pmtz ligands involved in both $\mu\text{-}\eta^1(N),\eta^2(N,N)$ and orthometalated $\mu\text{-}\eta^1(C),\eta^2(N,N)$ bonding modes, was prepared by substitution of a bridging acetate in the parent $Ru_3O(OAc)_6$ cluster core. Chemical or electrochemical reduction or oxidation of $[\mathbf{5}]^{2+}$ gave one-electron reduced product $[\mathbf{5a}]^+$ or oxidized species $[\mathbf{5b}]^{3+}$, respectively. It is demonstrated that substitution of the bridging acetate by a triazine ligand has a remarkable impact on the electronic and redox characteristics of the triruthenium cluster derivatives. Electrochemical, UV/Vis/NIR spectra, and DFT computational studies demonstrated that there is a distinct cluster–cluster interaction between the two triruthenium cluster moieties across an asymmetric bridging bis(tridentate) triazine in the dimeric triruthenium cluster complex $[\mathbf{5}]^{2+}$.

Introduction

Over the years considerable attention has been paid to multinuclear transition-metal complexes that exhibit multiple redox processes and ligand-mediated electronic interactions because they are attractive as new multifunctional materials.[1–4] For example, these functional complexes have potential applications in catalysis, photo/electroluminescence, nonlinear optics, and molecular devices.[5–9]

Oxo-centered trinuclear ruthenium–carboxylate cluster compounds with general formula $[Ru_3O(OAc)_6(L)(L')(L'')]^n$ (L, L′, and L′ = axial ligand, n = 0, 1, 2) are promising building blocks in view of their rich substitution reactivity, multiple redox behavior, diverse mixed-valence chemistry, and intriguing catalytic properties.[10–21] Owing to their comparative lability, axial ligand substitution affords an excellent means to tune the redox levels of electron-transfer processes and enhances significantly the richness of triruthenium chemistry.[11–16,22–24] A number of oligomeric triruthenium cluster derivatives linked by pyrazine, 4,4′-bipyridine, polyphosphane, and polypyridyl ligands have been synthesized and characterized,[10–15] and the electronic communication between the triruthenium moieties has been examined.

Compared with axial ligand substitution, displacement of a bridging acetate in the parent triruthenium cluster core $Ru_3(\mu_3\text{-}O)(\mu\text{-}OAc)_6$ is much more difficult to achieve.[14,25–27] In an attempt to explore the reactivity of the $Ru_3^{III,III,III}$ precursor $[Ru_3O(OAc)_6(py)_2(CH_3OH)]^+$ ($[\mathbf{1}]^+$) with 2,2′-bipyridine, we successfully isolated $[Ru_3O(OAc)_5\{\mu\text{-}\eta^1(C),\eta^2(N,N)\text{-bipyridine}\}(py)_2]^+$ by substitution of a bridging acetate in the parent triruthenium core $Ru_3(\mu_3\text{-}O)(\mu\text{-}OAc)_6$ by an *ortho*-metalated 2,2′-bipyridine.[25,26] Subsequently, a series of low-valence (III,III,II or III,II,II) triruthenium derivatives were prepared by substitution of a bridging acetate by a π-delocalized neutral N-heterocyclic ligand with a low-lying π* orbital and strong π-accepting character.[27] Although substitution of a bridging acetate by an anionic polypyridyl ligand by *ortho*-metalation exerts little influence on the physicochemical properties,[25,26] substitution of a bridging acetate by a neutral N-heterocyclic ligand significantly affects the electronic and redox characteristics of oxo-centered triruthenium cluster derivatives.[27]

In this paper we wish to report the synthesis of dimeric triruthenium cluster derivatives by bridging ligand substitution using a symmetric bis(tridentate) ligand with two identical $\mu\text{-}\eta^1(N),\eta^2(N,N)$ donors or an asymmetric bis(tridentate) ligand that adopts both $\mu\text{-}\eta^1(N),\eta^2(N,N)$ and *ortho*-metalated $\mu\text{-}\eta^1(C),\eta^2(N,N)$ bonding modes. 5,5′,6,6′-Tetramethyl-3,3′-bi-1,2,4-triazine (bdmt) was selected as a potential symmetric bis[$\mu\text{-}\eta^1(N),\eta^2(N,N)$] bridging ligand and 3-(2-pyrimidinyl)-1,2,4-triazine (pmtz) served as an asymmetric bis(tridentate) ligand that affords both μ-

[a] State Key Laboratory of Structural Chemistry, Fujian Institute of Research on the Structure of Matter, Chinese Academy of Sciences,
Fujian 350002, P. R. China
E-mail: czn@fjirsm.ac.cn

Supporting information for this article is available on the WWW under http://dx.doi.org/10.1002/ejic.201100093.

η^1(N),η^2(N,N) and η^1(C),η^2(N,N) donors, thereby creating an efficient approach to triruthenium cluster–cluster electronic interaction. Although isolation of the dimeric triruthenium cluster complex with symmetric bis(tridentate) bdmt is unattainable, asymmetric bis(tridentate) pmtz-linked dimeric species $[\{Ru_3O(OAc)_5(py)_2\}_2\{\mu_4\text{-}\eta^1(C),\eta^1(N),\eta^2(N,N),\eta^2(N,N)\text{-pmtz}\}]^{n+}$ (n = 1, 2, or 3) with three different charges have been obtained as anticipated. We describe herein spectroscopic, redox, and DFT computational studies of these monomeric and dimeric triruthenium cluster derivatives.

Results and Discussion

Syntheses and Characterization

The synthetic routes to triruthenium cluster complexes $[\mathbf{2}]^+$–$[\mathbf{5}]^{3+}$ are summarized in Scheme 1. Monomeric $[Ru_3^{III,III,II}]^+$ cluster complexes $[\mathbf{2}]^+$–$[\mathbf{4}]^+$ were synthesized by the reaction of the $[Ru_3^{III,III,III}]^+$ precursor $[\mathbf{1}]^+$ with 1.2 equiv. of pytz, bdmt, or pmtz at room temperature, respectively. The products were purified by chromatography on alumina columns. The stable $[Ru_3^{III,III,II}]^+$ cluster derivatives $[\mathbf{2}]^+$–$[\mathbf{4}]^+$ are formed by one-electron reduction of valence III,III,III to III,III,II and by substitution of a bridging acetate and an axially coordinated methanol in the $Ru_3^{III,III,III}$ precursor $[\mathbf{1}]^+$ by pytz, bdmt, or pmtz, with pytz, bdmt, and pmtz adopting the μ-η^1(N),η^2(N,N) bonding mode.

When the molar ratio of $[\mathbf{1}]^+$ and pmtz was 2.2:1, the main product isolated was the pmtz-linked dimeric complex $[\mathbf{5}]^{2+}$ ($Ru_3^{III,III,II}$–pmtz–$Ru_3^{III,III,III}$) with intercluster mixed-valence. Dimeric complex $[\mathbf{5}]^{2+}$ was also accessible by the reaction of $[\mathbf{4}]^+$ with 1 equiv. of $[\mathbf{1}]^+$. The pmtz-linked dimeric complex $[\mathbf{5}]^{2+}$ consists of two $Ru_3O(OAc)_5(py)_2$ units with formal oxidation states III,III,II and III,III,III, respectively, in which the pmtz is bound to the former $Ru_3^{III,III,II}O(OAc)_5(py)_2$ moiety in a η^1(N),η^2(N,N) bonding mode and the latter in a η^1(C),η^2(N,N) bonding mode by *ortho*-metalation. Electrochemical or chemical reduction of the 2+ species $[\mathbf{5}]^{2+}$ with an excess of aqueous hydrazine afforded the 1+ species $[\mathbf{5a}]^+$ ($Ru_3^{III,III,II}$–pmtz–$Ru_3^{III,III,II}$), which contains two identical $Ru_3O(OAc)_5(py)_2$ moieties with formal oxidation state III,III,II. On the other hand, electrochemical or chemical oxidation of $[\mathbf{5}]^{2+}$ with 1 equiv. of ferrocenium hexafluorophosphate gave the 3+ species

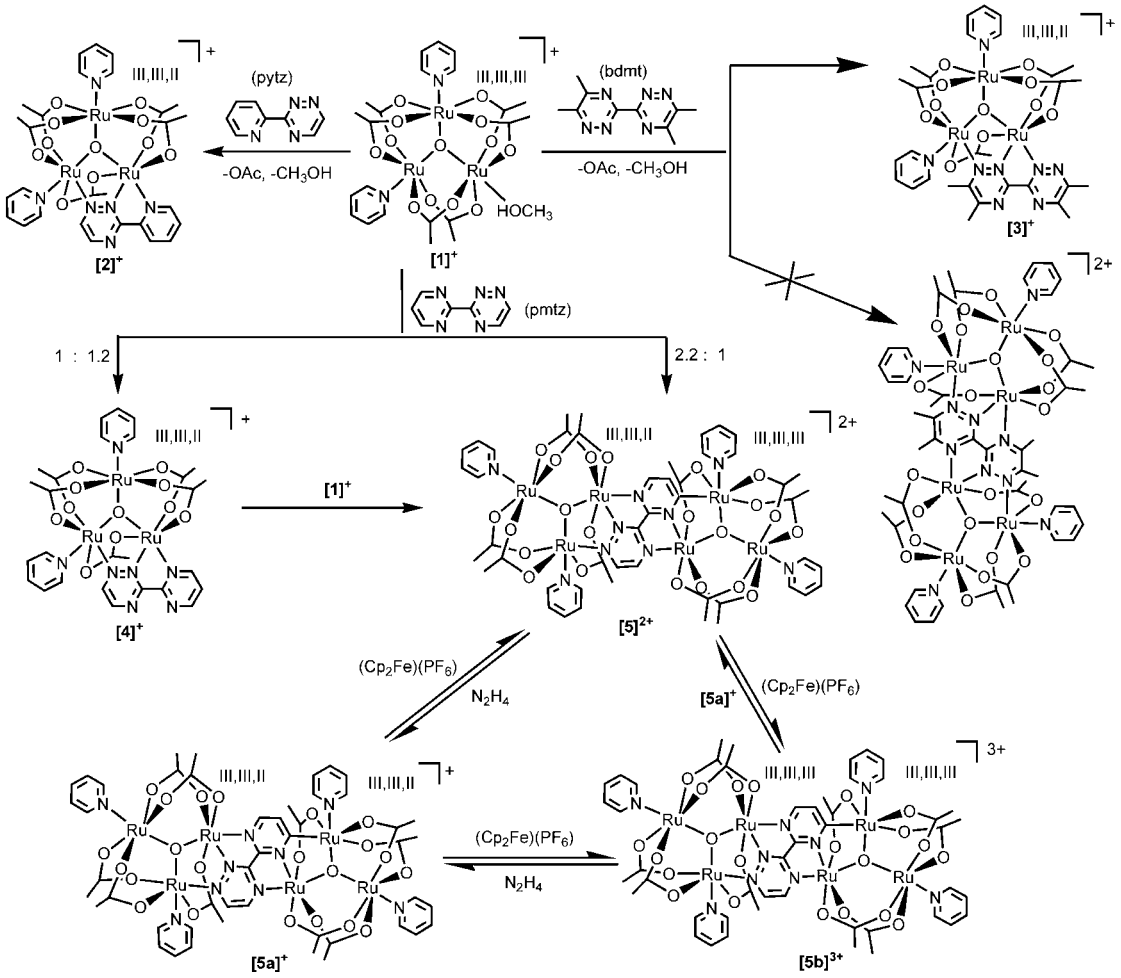

Scheme 1. Synthesis of $[\mathbf{2}]^+$–$[\mathbf{5b}]^{3+}$.

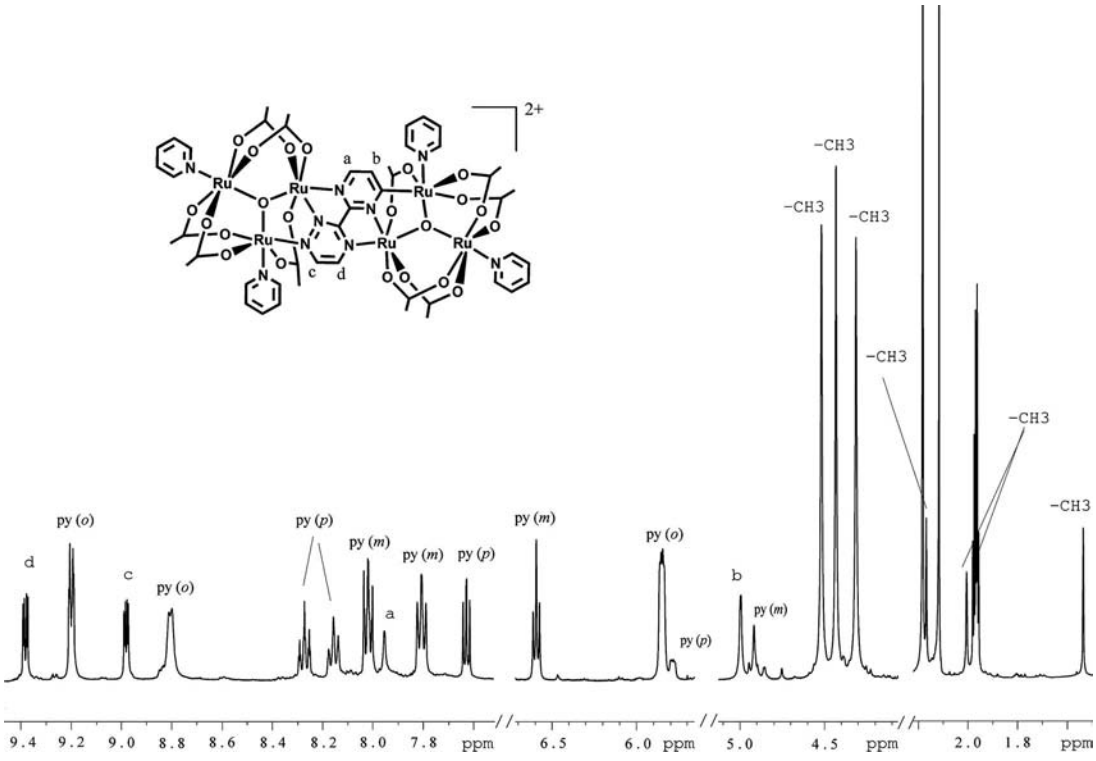

Figure 1. ^{1}H NMR (400 MHz) spectrum of complex $[\mathbf{5}]^{2+}$ in CD_3CN.

$[\mathbf{5b}]^{3+}$ ($Ru_3^{III,III,III}$–pmtz–$Ru_3^{III,III,III}$) containing two identical $Ru_3O(OAc)_5(py)_2$ moieties with formal oxidation state III,III,III.

The reaction of bdmt with 2.2 equiv. of $[\mathbf{1}]^+$ afforded simply the monomeric triruthenium derivative $[\mathbf{3}]^+$. The attempt to access the desired dimeric triruthenium species (Scheme 1) with bis[η^1(N),η^2(N,N)]-bdmt failed, probably due to the greater stability of $[\mathbf{3}]^+$ with η^1(N),η^2(N,N)-bdmt compared with that of the dimeric species with bis[η^1(N),η^2(N,N)]-bdmt.

Complexes $[\mathbf{2}]^+$–$[\mathbf{5b}]^{3+}$ were characterized by elemental analysis, ESI-MS spectrometry, UV/Vis/NIR, IR, and ^{1}H NMR spectroscopy, and cyclic and differential pulse voltammetry. The elemental analyses (C, H, N) coincided well with the calculated values for all the compounds. Positive ion ES-MS of $[\mathbf{2}]^+$, $[\mathbf{3}]^+$, $[\mathbf{4}]^+$, $[\mathbf{5a}]^+$, $[\mathbf{5}]^{2+}$, and $[\mathbf{5b}]^{3+}$ (Figures S1–6, Supporting Information) showed the corresponding molecular ion fragments [M – PF_6]$^+$, [M – $2PF_6$]$^{2+}$, or [M – $3PF_6$]$^{3+}$ as the base or principal peaks, respectively.

The ^{1}H NMR spectroscopic data for complexes $[\mathbf{2}]^+$–$[\mathbf{5}]^{2+}$ together with the tentative assignments are collected in Table S1 (Supporting Information) for the purpose of comparison. The ^{1}H NMR spectra are presented in Figure 1 for $[\mathbf{5}]^{2+}$ and Figures S7–S9 (see Supporting Information) for $[\mathbf{2}]^+$–$[\mathbf{4}]^+$, respectively. Complexes $[\mathbf{2}]^+$–$[\mathbf{4}]^+$ are diamagnetic, as evidenced by the ^{1}H NMR spectroscopic data, with the proton signals tentatively assigned by reference to relevant oxo-centered triruthenium cluster complexes reported in the literature.[22–27] The 2+ dimeric complex $[\mathbf{5}]^{2+}$, however, showed a clear paramagnetic shift relative to that of the diamagnetic monomeric complex $[\mathbf{4}]^+$ due to the influence of an unpaired electron. As shown in Figure 1, the acetate methyl protons of paramagnetic $[\mathbf{5}]^{2+}$ are observed in the range 1.53–4.52 ppm, in striking contrast to those of diamagnetic $[\mathbf{4}]^+$ (1.56–2.42 ppm; Figure S9, Supporting Information). The proton signals of two pyridine ligands in $[\mathbf{5}]^{2+}$ are clearly shifted to higher fields compared with those in $[\mathbf{4}]^+$ with diamagnetism, which shows effective paramagnetic shifts.

Crystal Structures

The structures of $[\mathbf{2}](PF_6)\cdot CH_2Cl_2$, $[\mathbf{3}](PF_6)\cdot 3CH_2Cl_2$, and $[\mathbf{4}](PF_6)\cdot \frac{1}{2}CH_2Cl_2\cdot H_2O$ were determined by single-crystal X-ray diffraction. Selected bond lengths and angles are summarized in Table 1. The ORTEP drawing of $[\mathbf{4}]^+$ is depicted in Figure 2.

The pytz, bdmt, and pmtz ligands exhibit a μ-η^1(N),η^2(N,N) bonding mode, which is favored by the formation of two five-membered coordination rings. Note that the axial Ru1–N1 [2.064(4)–2.089(5) Å] distance within the five-membered chelating ring is markedly longer than the equatorial Ru1–N2 [1.919(8)–1.951(4) Å] bond.[14,27] The chelating effect induces a shorter axial Ru1–N1 [2.064(4)–2.089(5) Å] length than the other two axial Ru–N_{py} [2.089(7)–2.157(9) Å] bonds. The two N-heterocyclic rings in the pytz, bdmt, and pmtz ligands are almost coplanar with an angle of 4.5° for $[\mathbf{2}]^+$, 7.4° for $[\mathbf{3}]^+$, and 10.1° for $[\mathbf{4}]^+$.

As a result of the μ-η^1(N),η^2(N,N) bonding mode of pytz, bdmt, and pmtz, the triruthenium frameworks form

Table 1. Selected bond lengths [Å] and angles [°] for [**2**](PF_6)·CH_2Cl_2, [**3**](PF_6)·$3CH_2Cl_2$, and [**4**](PF_6)·$½CH_2Cl_2$·H_2O.

	[**2**](PF_6)·CH_2Cl_2		[**3**](PF_6)·$3CH_2Cl_2$		[**4**](PF_6)·$½CH_2Cl_2$·H_2O			
Ru···Ru	Ru1···Ru2	3.232(4)	Ru1···Ru2	3.227(3)	Ru1···Ru2	3.226(7)	Ru4···Ru5	3.225(8)
	Ru1···Ru3	3.346(5)	Ru1···Ru3	3.348(4)	Ru1···Ru3	3.337(7)	Ru4···Ru6	3.332(7)
	Ru2···Ru3	3.363(3)	Ru2···Ru3	3.340(4)	Ru2···Ru3	3.343(8)	Ru5···Ru6	3.358(9)
Ru–$O_{central}$	Ru1–O1	1.915(4)	Ru1–O1	1.925(3)	Ru1–O1	1.935(6)	Ru4–O12	1.926(6)
	Ru2–O1	1.944(4)	Ru2–O1	1.928(3)	Ru2–O1	1.934(7)	Ru5–O12	1.920(6)
	Ru3–O1	1.889(4)	Ru3–O1	1.878(3)	Ru3–O1	1.860(6)	Ru6–O12	1.884(6)
Ru–N	Ru1–N1	2.089(5)	Ru1–N1	2.064(4)	Ru1–N1	2.062(9)	Ru4–N8	2.065(9)
	Ru1–N2	1.944(5)	Ru1–N2	1.951(4)	Ru1–N2	1.920(10)	Ru4–N9	1.919(8)
	Ru2–N3	1.979(5)	Ru2–N3	2.040(4)	Ru2–N3	1.998(10)	Ru5–N10	1.972(8)
	Ru3–N5	2.126(5)	Ru2–N7	2.114(4)	Ru2–N6	2.089(7)	Ru5–N13	2.106(8)
	Ru2–N6	2.106(5)	Ru3–N8	2.123(4)	Ru3–N7	2.157(9)	Ru6–N14	2.143(8)
Ru–$O_{central}$–Ru	Ru1–O1–Ru2	113.7(2)	Ru1–O1–Ru2	113.75(15)	Ru1–O1–Ru2	112.9(3)	Ru4–O12–Ru5	113.9(3)
	Ru1–O1–Ru3	123.2(2)	Ru1–O1–Ru3	123.33(15)	Ru1–O1–Ru3	123.2(4)	Ru4–O12–Ru6	121.9(3)
	Ru2–O1–Ru3	122.7(2)	Ru2–O1–Ru3	122.71(16)	Ru2–O1–Ru3	123.5(3)	Ru5–O12–Ru6	123.9(3)
N–Ru–$O_{central}$	N1–Ru1–O1	166.96(19)	N1–Ru1–O1	168.12(14)	N1–Ru1–O1	172.0(3)	N8–Ru4–O12	170.6(3)
	N2–Ru1–O1	89.14(19)	N2–Ru1–O1	89.03(14)	N2–Ru1–O1	90.4(3)	N9–Ru4–O12	90.4(3)
	N3–Ru2–O1	88.54(19)	N3–Ru2–O1	88.75(13)	N3–Ru2–O1	88.2(4)	N10–Ru5–O12	90.3(3)
	N5–Ru2–O1	179.0(2)	N7–Ru2–O1	174.25(14)	N6–Ru2–O1	178.0(3)	N13–Ru5–O12	179.3(3)
	N6–Ru3–O1	178.02(19)	N8–Ru3–O1	179.01(15)	N7–Ru3–O1	179.5(3)	N14–Ru6–O12	178.0(3)
N–Ru–N	N1–Ru1–N2	79.1(2)	N1–Ru1–N2	79.36(15)	N1–Ru1–N2	81.9(4)	N8–Ru4–N9	80.5(3)
	N3–Ru2–N6	92.7(2)	N3–Ru2–N7	96.52(15)	N3–Ru2–N6	90.0(4)	N10–Ru5–N13	89.9(3)

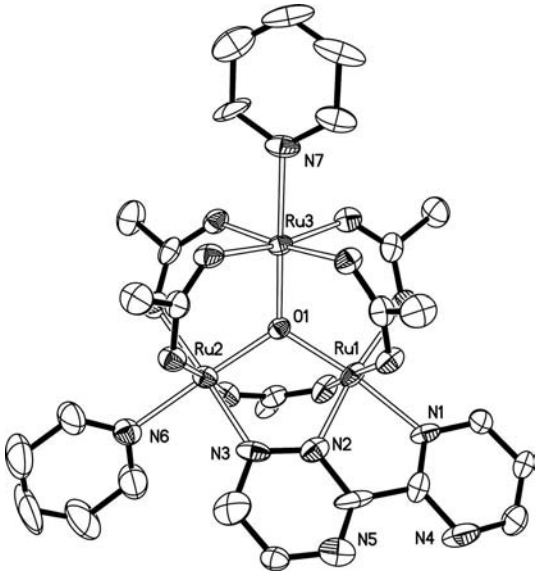

Figure 2. ORTEP drawing of [**4**]$^+$. Tthermal ellipsoids are drawn at the 30% probability level.

approximately isosceles triangles with Ru1···Ru2 distances [3.226(7)–3.232(4) Å] distinctly shorter than those of Ru1···Ru3 [3.337(7)–3.348(4) Å] and Ru2···Ru3 [3.340(4)–3.363(3) Å]. The Ru1–O1 and Ru2–O1 [1.915(4)–1.944(4) Å] distances are clearly longer than the Ru3–O1 distances [1.860(6)–1.889(4) Å]. The Ru–$O_{acetate}$ distances [2.034(8)–2.093(4) Å] are comparable to those observed in other oxo-centered triruthenium cluster compounds.[22–27]

Electronic Absorption Properties

The electronic absorption spectroscopic data of [**2**]$^+$–[**5b**]$^{3+}$ in dichloromethane solutions at 298 K are summarized in Table 2. The intense bands in the UV region are dominated by ligand-centered absorptions arising from the $\pi \rightarrow \pi^*$ transitions of the aromatic rings. Based on the band assignments of similar triruthenium complexes[13,16,22–27] together with DTF computational results (see below), the series of composite bands of intermediate energy observed at 310–550 nm can be attributed to cluster-to-ligand charge-transfer (CLCT) transitions from the occupied 4d orbitals of the triruthenium cluster to the lowest-unoccupied π^* orbitals of the N or O ligand. This assignment is supported by the sensitivity of these bands to variations in the organic ligands.

Table 2. UV/Vis absorption spectroscopic data for compounds [**2**]PF_6–[**5b**](PF_6)$_3$ in dichloromethane.

	λ_{max} [nm] (ε [$dm^3 mol^{-1} cm^{-1}$])		
	IC[a]	CLCT[b]	Ligand-centered transitions
[**2**](PF_6)	652 (9800)	330 (14200)	241 (36700)
		457 (13400)	273 (25700)
		539 (11200)	
[**3**](PF_6)	653 (12900)	329sh (14600)	244 (46300)
		434 (17400)	
		540(14700)	
[**4**](PF_6)	647 (11300)	318 (13800)	242 (46700)
		396 (12100)	
		466 (13900)	
		533 (11900)	
[**5**](PF_6)$_2$	723 (15400)	333sh (21900)	238 (52600)
		551 (12000)	
[**5a**](PF_6)	861 (15600)	390 (22500)	247 (57500)
[**5b**](PF_6)$_3$	694 (15300)	335 (25900)	241 (56600)

[a] IC is an intracluster transition. [b] CLCT is a cluster-to-ligand charge-transfer transition.

The low-energy broad absorption bands centered at 640–860 nm can be assigned to intracluster (IC) transitions, as demonstrated by our DFT computational studies (see below). According to the qualitative molecular orbital scheme,[11,15,28] the variations in the electron contents or

formal oxidation states of the triruthenium clusters would cause noticeably red- or blueshifted low-energy IC bands. As shown in Figure 3, compared with the low-energy band in the 2+ complex $[\mathbf{5}]^{2+}$ (723 nm), the absorption due to IC transitions is significantly redshifted in the 1+ species $[\mathbf{5a}]^{+}$ (861 nm), whereas that of the 3+ complex $[\mathbf{5b}]^{3+}$ (694 nm) is clearly blueshifted. The decrease in energy of these transitions by stepwise one-electron reduction reflects a gradual increase in the occupied dπ levels as the electron number increases.[13,15,28] It is intriguing that compared with the monomeric complex $[\mathbf{4}]^{+}$ (647 nm), the IC bands (Figure 3) of the dimeric species $[\mathbf{5a}]^{+}$ (861 nm), $[\mathbf{5}]^{2+}$ (723 nm), and $[\mathbf{5b}]^{3+}$ (694 nm) shift significantly to a lower energy. As shown in Figure 3, the remarkable redshift of the intracluster charge-transfer (IC) bands from monomeric complex $[\mathbf{4}]^{+}$ to dimeric species $[\mathbf{5a}]^{+}$–$[\mathbf{5b}]^{3+}$ suggests that a strong cluster–cluster interaction most likely operates between the two triruthenium cluster moieties across the bridging pmtz in $[\mathbf{5a}]^{+}$–$[\mathbf{5b}]^{3+}$, as demonstrated by electrochemical and DFT studies (see below).[15,26]

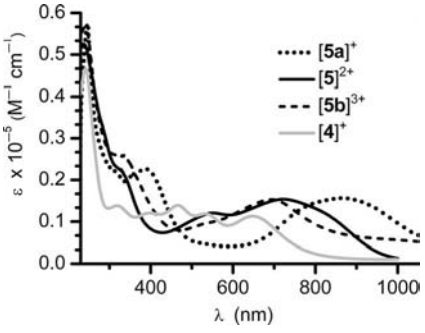

Figure 3. UV/Vis/NIR absorption spectra of $[\mathbf{4}]^{+}$ (grey), $[\mathbf{5}]^{2+}$ (solid), $[\mathbf{5a}]^{+}$ (dots), and $[\mathbf{5b}]^{3+}$ (dashes) in dichloromethane solution.

Redox Properties

The redox chemistry of $[\mathbf{2}]^{+}$–$[\mathbf{5}]^{2+}$ was investigated by cyclic and differential pulse voltammetry. The electrochemical data are summarized in Table 3 together with those of relevant oxo-centered triruthenium complexes for the purpose of comparison. Plots of cyclic and differential pulse voltammograms in 0.1 M acetonitrile solutions of $(Bu_4N)(PF_6)$ at ambient temperature are shown in Figure 4 for $[\mathbf{4}](PF_6)$ and $[\mathbf{5}](PF_6)_2$, and in Figure S14 (see Supporting Information) for $[\mathbf{2}](PF_6)$ and $[\mathbf{3}](PF_6)$. For monomeric triruthenium complexes $[\mathbf{2}]^{+}$–$[\mathbf{4}]^{+}$, four to five distinct reversible or quasi-reversible redox couples are detected in the potential range of +1.5 to –2.5 V vs. Fc/Fc^{+}, with waves A and B occurring in the anodic range and waves C, D, and E in the cathodic range. The quasi-reversible wave E (Figure S14, Supporting Information) is ascribable to the ligand-centered reduction (L/L^{-1}) because the free ligand undergoes the same reduction process at a similar potential under the same conditions of measurement. With reference to previous studies of

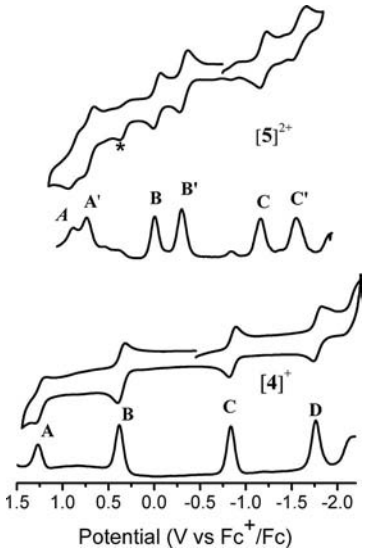

Figure 4. Cyclic and differential pulse voltammograms for compounds $[\mathbf{4}](PF_6)$ and $[\mathbf{5}](PF_6)_2$ in 0.1 M dichloromethane solutions of $(Bu_4N)(PF_6)$. Scan rates: 100 mV/s for CV and 20 mV/s for DPV. *A flaw of the instrument.

Table 3. Electrochemical data for compounds $[\mathbf{2}]PF_6$–$[\mathbf{5}](PF_6)_2$.[a]

	$E_{1/2}$(A) [V] ($Ru_3^{III,III,IV}$/ $Ru_3^{III,III,III}$)	$E_{1/2}$(B) [V] ($Ru_3^{III,III,III}$/ $Ru_3^{III,III,II}$)	$E_{1/2}$(C) [V] ($Ru_3^{III,III,II}$/ $Ru_3^{III,II,II}$)	$E_{1/2}$(D) [V] ($Ru_3^{III,II,II}$/ $Ru_3^{II,II,II}$)	$E_{1/2}$(E) [V] (L/L^{-1})
$[\mathbf{2}](PF_6)$	+1.19	+0.31	–0.92	–1.91	
$[\mathbf{3}](PF_6)$	+1.16	+0.27	–0.88	–1.77	2.12
$[\mathbf{4}](PF_6)$	+1.24	+0.36	–0.86	–1.78	
$[\mathbf{5}](PF_6)_2$	+0.87[b]	–0.03[b]	–1.19[b]		
	+0.71[c]	–0.32[c]	–1.58[c]		
$[Ru_3O(OAc)_5(bpy)(py)_2](PF_6)$[d]	+0.57	–0.57	–1.90		
$[Ru_3O(OAc)_6(py)_3](PF_6)$	+0.59	–0.60	–1.99		
$[Ru_3O(OAc)_6(py)_2CO]$[e]	+0.89	+0.25	–1.25		
$[Ru_3O(OAc)_6(CNXy)_3]$[f]	+0.94	–0.01	–0.67	–1.19	
$[Ru_3O(OAc)_5(abcp)(py)_2](PF_6)$[g]	+1.29	+0.53	–0.46	–1.58	
$[Ru_3O(OAc)_5(abpy)(py)_2](PF_6)$[g]	+1.14	+0.36	–0.76	–1.84	
$[Ru_3O(OAc)_5(cppd)(py)_2](PF_6)$[h]	+1.12	+0.19	–1.00	–1.87	–2.05

[a] Potential data in volts vs. Fc/Fc^{+} ($E_{1/2}$ = 0) are from single scan cyclic voltammograms recorded at 25 °C. Detailed experimental conditions are given in the Exp. Sect. [b] Redox processes due to the $\eta^1(N),\eta^2(N,N)$-bonded $Ru_3O(OAc)_5(py)_2$ unit. [c] Redox processes due to the $\eta^1(C),\eta^2(N,N)$-bonded $Ru_3O(OAc)_5(py)_2$ unit. [d] Data from ref.[25a] [e] Data from ref.[11] [f] Data from ref.[22] [g] Data from ref.[27a] [h] Data from ref.[27b]

a series of μ-η¹(N),η²(N,N)-ligand-substituted oxo-centered triruthenium species containing π-delocalized neutral N-heterocyclic ligands with a low π* level and strong π-accepting character,[27] waves A, B, C, and D correspond most probably to the successive one-electron redox processes $Ru_3^{IV,III,III}/Ru_3^{III,III,III}$ [$E_{1/2}$(A)], $Ru_3^{III,III,III}/Ru_3^{III,III,II}$ [$E_{1/2}$(B)], $Ru_3^{III,III,II}/Ru_3^{III,II,II}$ [$E_{1/2}$(C)], and $Ru_3^{III,II,II}/Ru_3^{II,II,II}$ [$E_{1/2}$(D)], respectively. As indicated in Table 3, compared with the parent complex $[Ru_3O(OAc)_6(py)_3]^+$,[15,27a] $E_{1/2}$(A), $E_{1/2}$(B), $E_{1/2}$(C), and $E_{1/2}$(D) in $[\mathbf{2}]^+$–$[\mathbf{5}]^{2+}$ are all remarkably positively shifted (0.57–1.13 V). This further demonstrates that substitution of a bridging acetate in the parent triruthenium cluster core $Ru_3(\mu_3\text{-}O)(\mu\text{-}OAc)_6$ by a neutral bridging N-heterocyclic ligand with a low π* level exerts significant influence on the redox properties in the triruthenium derivatives produced.

The cyclic voltammogram of $[\mathbf{5}]^{n+}$ (n = 1, 2, or 3) in a 0.1 M dichloromethane solution of $(Bu_4N)(PF_6)$ shows six reversible or quasi-reversible one-electron redox waves in the range of +1.0 to –1.6 V versus Fc/Fc^+. As depicted in Figure 4, the redox waves can be assigned by comparison with those of the monomeric complex $[\mathbf{4}]^+$ containing pmtz in the η¹(N),η²(N,N) bonding mode and with those of $[Ru_3O(OAc)_5(py)_2\{\mu\text{-}\eta^1(C),\eta^2(N,N)\text{-bpy}\}]^+$ with *ortho*-metalated bpy in the η¹(C),η²(N,N) bonding mode.[25] On going from +1.0 to –1.6 V, successive redox waves can be ascribed to the processes $[Ru_3^{IV,III,III}\text{–pmtz–}Ru_3^{IV,III,III}]^{5+}/[Ru_3^{III,III,III}\text{–pmtz–}Ru_3^{IV,III,III}]^{4+}$ (A), $[Ru_3^{III,III,III}\text{–pmtz–}Ru_3^{IV,III,III}]^{4+}/[Ru_3^{III,III,III}\text{–pmtz–}Ru_3^{III,III,III}]^{3+}$ (A′), $[Ru_3^{III,III,III}\text{–pmtz–}Ru_3^{III,III,III}]^{3+}/[Ru_3^{III,III,II}\text{–pmtz–}Ru_3^{III,III,III}]^{2+}$ (B), $[Ru_3^{III,III,II}\text{–pmtz–}Ru_3^{III,III,III}]^{2+}/[Ru_3^{III,III,II}\text{–pmtz–}Ru_3^{III,III,II}]^{+}$ (B′), $[Ru_3^{III,III,II}\text{–pmtz–}Ru_3^{III,III,II}]^{+}/[Ru_3^{III,II,II}\text{–pmtz–}Ru_3^{III,III,II}]^{0}$ (C), and $[Ru_3^{III,II,II}\text{–pmtz–}Ru_3^{III,III,II}]^{0}/[Ru_3^{III,II,II}\text{–pmtz–}Ru_3^{III,II,II}]^{-}$ (C′), respectively. It has been revealed that redox potentials of oxo-centered triruthenium complexes with a neutral bridging N-heterocyclic ligand are always more positive than those of oxo-centered triruthenium derivatives with an *ortho*-metalated anionic polypyridyl ligand.[14,25,27] Thus, waves A, B, and C are most likely due to the $Ru_3O(OAc)_5(py)_2$ moiety bound to η¹(N),η²(N,N) donors whereas waves A′, B′, and C′ probably arise from the other $Ru_3O(OAc)_5(py)_2$ unit bonded to *ortho*-metalated η¹(C),η²(N,N) donors.[25,27]

Direct comparison of the potential differences $\Delta E_{1/2}$ between waves A and A′ (0.16 A), B and B′ (0.29 V), and C and C′ (0.39 V) cannot give a precise estimation of cluster–cluster electronic interactions in asymmetric dimeric complexes $[\mathbf{5}]^{n+}$. Nevertheless, the corresponding potential differences (0.33–0.39 V) between waves A, B and C of monomeric complex $[\mathbf{4}]^+$ containing neutral pmtz and waves A, B, and C in dimeric species $[\mathbf{5}]^{n+}$ due to the $Ru_3O(OAc)_5(py)_2$ moiety bound to η¹(N),η²(N,N) donors may give useful information to estimate Ru_3–pmtz–Ru_3 intercluster interactions. The significant negative potential shifts (0.33–0.39 V) from monomeric complex $[\mathbf{4}]^+$ to dimeric species $[\mathbf{5}]^{n+}$ are most likely due to a substantial cluster–cluster interaction between two $Ru_3O(OAc)_5(py)_2$ moieties across bridging pmtz.[29] Such a cluster–cluster electronic interaction in dimeric complexes $[\mathbf{5}]^{n+}$ with asymmetric bis(tridentate) pmtz is likely comparable to that in dimeric triruthenium cluster complexes $[\{Ru_3O(OAc)_5(py)_2\}_2\{\mu_4\text{-}\eta^1(C),\eta^1(C),\eta^2(N,N),\eta^2(N,N)\text{-bpym}\}]^{n+}$ (n = 0, 1, or 2) with symmetric bis(*ortho*-metalated) 2,2′-bipyrimidine.[26]

Electronic Structures and DFT Computational Studies

To elucidate the interactions between two cluster moieties in dimeric complexes $[\mathbf{5}]^{2+}$, density functional theory (DFT) was used to study the electronic structures of complexes $[\mathbf{2}]^+$, $[\mathbf{4}]^+$, $[\mathbf{5a}]^+$, and $[\mathbf{5}]^{2+}$. On the basis of their optimized geometries, 60 singlet and 6 triplet excited states of related complexes were calculated at the LanL2DZ[6-31G(d)] level of theory by TD-DFT, in which the solvent effect (CH_2Cl_2 as the solvent) was taken into account by using the PCM approach. The relative compositions of the different energy levels in terms of the constituent fragments and the absorption transition characters are summarized in Table 4 for $[\mathbf{4}]^+$, Table 5 for $[\mathbf{5}]^{2+}$, Tables S3 and S4 for $[\mathbf{2}]^+$, and Tables S5 and S6 for $[\mathbf{5a}]^+$ (for the latter, see Supporting Information). The electron-density diagrams of the frontier molecular orbitals involved in the absorption spectra are depicted in Figure 5 for $[\mathbf{5a}]^+$ and Figures S17–S19 for $[\mathbf{2}]^+$, $[\mathbf{4}]^+$, and $[\mathbf{5}]^{2+}$, respectively.

The HOMOs of triruthenium complexes $[\mathbf{2}]^+$ and $[\mathbf{4}]^+$ are mainly resident on ruthenium atoms (72.4–81.5% for $[\mathbf{2}]^+$ and 65.0–81.2% for $[\mathbf{4}]^+$) with a minor distribution on the acetates (10.8–22.6% for $[\mathbf{2}]^+$ and 7.7–22.7% for $[\mathbf{4}]^+$). The LUMO is primarily on the ruthenium atoms (66.3% for $[\mathbf{2}]^+$ and 66.1% for $[\mathbf{4}]^+$) and the μ_3-O atom (22.1% for $[\mathbf{2}]^+$ and 22.0% for $[\mathbf{4}]^+$). Note that triazine ligands pytz and pmtz make a major contribution to the LUMO+1, LUMO+2, and LUMO+3. In the case of LUMO+2, the triazine ligand character is 91.8% for $[\mathbf{2}]^+$ and 89.3% for $[\mathbf{4}]^+$. The calculated low-energy absorptions HOMO-2→LUMO and HOMO-3→LUMO for $[\mathbf{2}]^+$ (Table S4) and HOMO-1→LUMO and HOMO-2→LUMO for $[\mathbf{4}]^+$ (Table 4) are primarily typical of intracluster (IC) transitions between 4d orbitals within a Ru_3 cluster. The DFT calculated values (632 nm for $[\mathbf{2}]^+$ and 636 nm for $[\mathbf{4}]^+$) accord well with the measured low-energy absorption maxima at 652 nm for $[\mathbf{2}]^+$ and 647 nm for $[\mathbf{4}]^+$. The calculated absorptions HOMO-7→LUMO+2 at 399 nm for $[\mathbf{2}]^+$ and 414 nm for $[\mathbf{4}]^+$ can be ascribed to 4d(Ru_3)→π*(pytz or pmtz) cluster-to-ligand charge-transfer (CLCT) transitions, which coincide reasonably with the measured bands at 457 nm for $[\mathbf{2}]^+$ and 434 nm for $[\mathbf{4}]^+$.

The HOMO of $[\mathbf{5}]^{2+}$ is primarily resident on the left $Ru_3^{III,III,II}$ cluster bonded to η¹(N),η²(N,N) donors. The LUMO is mainly distributed on the right $Ru_3^{III,III,III}$ moiety bonded to η¹(C),η²(N,N) donors but is delocalized onto the bridging ligand pmtz and the left Ru_3O cluster. As presented in Table 5, the calculated low-energy HOMO→LUMO absorptions can be assigned to both intracluster (IC) and cluster–cluster (CC) transitions mixed

Table 4. Partial molecular orbital compositions in the ground state and the absorption transitions for $[\mathbf{4}]^+$ in dichloromethane calculated by the TD-DFT method.

Orbital	Energy [eV]	MO contribution [%]				
		Ru	pmtz	py	μ_3-O	OAc
LUMO+2	–3.1364	8.3	89.3	0.5	0.4	1.5
LUMO+1	–3.2202	15.9	81.9	0.3	0.1	1.8
LUMO	–3.9822	66.1	3.0	3.6	22.0	5.3
HOMO	–5.9199	72.1	2.4	1.6	1.0	22.7
HOMO-1	–6.1047	79.0	2.6	1.5	0.1	16.8
HOMO-2	–6.2160	80.3	2.4	3.1	0.9	13.3
HOMO-4	–6.4176	65.0	13.3	0.7	0.2	20.8
HOMO-6	–6.6075	78.0	8.3	2.5	3.5	7.7
HOMO-7	–6.6943	81.2	4.4	2.1	1.4	10.9

Transition	Transition	CI coefficient	*E* [nm] (eV)	Oscillation strength	Assignment	Measured value [nm]
S1	HOMO→LUMO	0.6127	1954 (0.63)	0.0000	^{1}IC	
S8	HOMO-2→LUMO	0.4050	636 (1.94)	0.0978	^{1}IC	647
	HOMO-1→LUMO	0.3148			^{1}IC	
S25	HOMO-7→LUMO+2	0.4426	414 (2.99)	0.1341	^{1}CLCT	434
	HOMO-6→LUMO+2	–0.2256			^{1}CLCT	
	HOMO-4→LUMO+1	0.2700			^{1}CLCT	

Table 5. Partial molecular orbital compositions in the ground state and the absorption transitions for $[\mathbf{5}]^{2+}$ in dichloromethane calculated by the TD-DFT method.

Orbital	Energy [eV]	MO contribution [%]								
		η^1(N),η^2(N,N)-$Ru_3^{III,III,II}$ unit				Bridging ligand pmtz	η^1(C),η^2(N,N)-$Ru_3^{III,III,III}$ unit			
		Ru	py	μ_3-O	OAc		Ru	py	μ_3-O	OAc
αLUMO+2	–3.7876	7.6	0.2	0.2	1.0	64.0	20.5	0.5	4.7	1.3
αLUMO+1	–4.0472	66.1	1.6	19.5	6.4	5.7	0.6	0.0	0.0	0.1
βLUMO+1	–4.0578	2.7	0.0	0.1	0.3	8.4	65.3	3.6	9.2	10.4
αLUMO	–4.3571	13.1	0.1	0.1	1.7	20.5	46.9	0.7	12.1	4.8
βLUMO	–4.3144	0.6	0.0	0.0	0.1	3.9	73.1	2.5	4.5	15.3
αHOMO	–6.2891	70.3	2.0	1.3	14.7	8.0	3.2	0.1	0.2	0.4
βHOMO	–6.3090	71.2	1.0	2.5	22.0	2.3	1.0	0.0	0.1	0.1
αHOMO-3	–6.7751	57.0	1.9	2.7	16.3	11.1	8.7	0.3	1.1	1.0
βHOMO-3	–6.6603	2.8	0.1	0.1	0.7	1.1	72.8	2.2	6.1	14.2
αHOMO-5	–6.8889	24.0	1.2	0.8	4.4	3.8	49.4	0.7	2.4	13.3
αHOMO-6	–6.9885	51.1	0.5	3.7	6.8	7.4	21.5	2.8	0.4	5.8
αHOMO-7	–7.0307	1.9	0.1	0.1	0.2	3.3	71.6	3.2	5.1	14.5
αHOMO-8	–7.0377	21.7	1.7	1.9	12.5	0.4	52.5	1.4	0.2	2.7

Transition	Transition	CI coef.	*E* [nm] (eV)	Oscillation strength	Assignment	Measured value [nm]
S1	βHOMO-3→βLUMO	0.8820	5444 (0.23)	0.0001	^{1}IC	
S6	αHOMO-5→αLUMO	0.4902	1898 (0.65)	0.0082	^{1}IC/^{1}CC	
	αHOMO→αLUMO	0.4830			^{1}IC/^{1}CC	
	αHOMO-8→αLUMO	0.3587			^{1}IC/^{1}CC	
S11	αHOMO→αLUMO	0.4023	1464 (0.85)	0.0056	^{1}IC/^{1}CC	
	αHOMO→αLUMO+2	0.3227			^{1}IC/^{1}CC	
	αHOMO-8→αLUMO	0.3127			^{1}IC/^{1}CC	
S15	βHOMO-3→βLUMO+1	0.6607	868 (1.43)	0.0319	^{1}IC	723
	βHOMO-3→βLUMO	–0.5012			^{1}IC	
	αHOMO-7→αLUMO	–0.3233			^{1}IC/^{1}CLCT/^{1}CC	
S19	αHOMO-7→αLUMO	0.4893	759 (1.63)	0.0308	^{1}IC/^{1}CLCT/^{1}CC	723
	αHOMO-3→αLUMO+1	–0.3108			^{1}IC	
	αHOMO-6→αLUMO	–0.2522			^{1}CC/^{1}CLCT	
	αHOMO-5→αLUMO	–0.2602			^{1}IC/^{1}CC	
	βHOMO→βLUMO	–0.2545			^{1}IC	

with a minor contribution from CLCT states. The calculated absorptions at 868 and 759 nm accord reasonably with the measured low-energy band with the maximum at 723 nm. When $[\mathbf{5}]^{2+}$ is photoexcited, the electron in the HOMO moves from the left $Ru_3^{III,III,II}$ cluster to the right $Ru_3^{III,III,III}$ cluster through the bridging pmtz, which implies that charge-transfer transitions between the two Ru_3 cluster moieties indeed operate in intercluster mixed-valence complex $[\mathbf{5}]^{2+}$ ($Ru_3^{III,III,II}$–pmtz–$Ru_3^{III,III,III}$) due to significant cluster–cluster interactions.

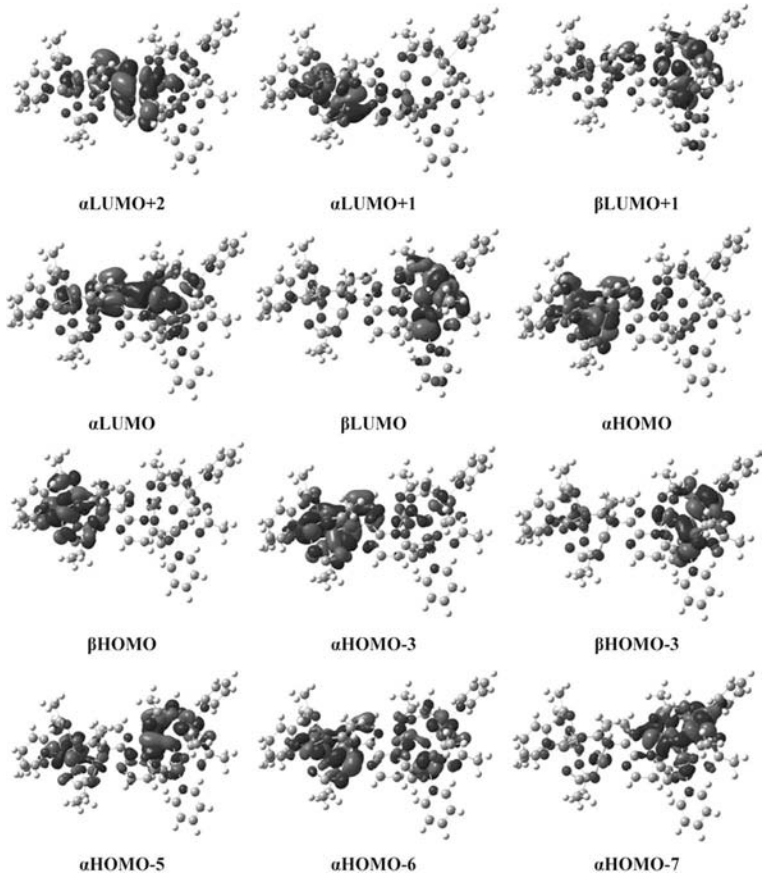

Figure 5. Electron density diagrams of the frontier molecular orbitals involved in the absorption of intercluster mixed-valence complex $[\mathbf{5}]^{2+}$ ($Ru_3^{III,III,II}$–pmtz–$Ru_3^{III,III,III}$).

The HOMO–LUMO gaps of the $Ru_3^{III,III,II}$ complexes $[\mathbf{2}]^+$ and $[\mathbf{4}]^+$, and $[\mathbf{5a}]^+$ composed of two $Ru_3^{III,III,II}$ units are 1.95, 1.94, and 1.47 eV, respectively. The interaction of the two $Ru_3^{III,III,II}$ cluster units in the dimeric complex $[\mathbf{5a}]^+$ leads to a distinct decrease in the HOMO–LUMO gap compared with in the monomeric complex $[\mathbf{4}]^+$. Upon one-electron oxidation of $[\mathbf{5a}]^+$ to $[\mathbf{5}]^{2+}$, the HOMO level in the dimeric complex $[\mathbf{5}]^{2+}$ containing one $Ru_3^{III,III,III}$ and one $Ru_3^{III,III,II}$ is significantly lowered, and thus the HOMO–LUMO gap is increased to 1.93 eV in $[\mathbf{5}]^{2+}$ relative to that of $[\mathbf{5a}]^+$ (1.47 eV). This suggests that loss of one electron from $[\mathbf{5a}]^+$ to $[\mathbf{5}]^{2+}$ results in a marked blueshift of the IC absorptions. As revealed from the UV/Vis spectra, the low-energy bands due to IC transitions occur at 861 nm for $[\mathbf{5a}]^+$ and 723 nm for $[\mathbf{5}]^{2+}$.

The charge population can be evidenced from a Mulliken population analysis, which is performed by using the GGA-PW91 functional of the CASTEP code based on the geometry structure optimized by Gaussian 03.[30] Tables S7 and S8 display the charges and bond populations of some selective atoms and bonds in $[\mathbf{4}]^+$, $[\mathbf{5a}]^+$, and $[\mathbf{5}]^{2+}$.

For complex $[\mathbf{4}]^+$, the calculated Mulliken charges of the Ru atoms in the Ru_3 core are considerably lower than the formal charge of $Ru_3^{III,III,II}$ and are found to be 1.50*e*, 1.57*e*, and 1.53*e*, and the total charge of the pmtz ligand is –1.85*e*. This suggests that the electrons are delocalized on the Ru_3 core and that there is a back-donation of electrons from the Ru_3 core to the pmtz ligand. In the intercluster mixed-valence dimeric complex $[\mathbf{5}]^{2+}$ ($Ru_3^{III,III,II}$–pmtz–$Ru_3^{III,III,III}$), the total charges of the two Ru_3 cores are 4.68*e* ($Ru_3^{III,III,II}$ core) and 4.70*e* ($Ru_3^{III,III,III}$ core). When $[\mathbf{5}]^{2+}$ is one-electron reduced to $[\mathbf{5a}]^+$, the total charges of the Ru_3 cores decrease from 4.68*e* and 4.70*e* to 4.52*e* and 4.47*e*, respectively. These results suggest that the electrons are delocalized over the Ru_3–pmtz–Ru_3 backbone and that electron communication indeed operates between the two Ru_3 cores through bridging ligand pmtz.

Conclusions

A series of triazine-substituted oxo-centered triruthenium derivatives have been obtained by displacing one of the six bridging acetates as well as an axial ligand in precursor triruthenium compound $[\mathbf{1}]^+$. These triazine-containing triruthenium complexes display large redox potential shifts to the anodic side because of bridging ligand substitution by a neutral triazine ligand with low-lying π* orbitals. For the dimeric species $[\mathbf{5}](PF_6)_2$, pmtz behaves as an asymmetrical bis(tridentate) ligand, adopting both μ-η^1(N),η^2(N,N) and μ-η^1(C), η^2(N,N) bonding modes to link two $Ru_3O(OAc)_5(py)_2$ cluster moieties. A significant cluster–cluster elec-

tronic interaction operates between the two triruthenium cluster moieties across the bridging pmtz ligand in the dimeric complexes $[\mathbf{5}]^{n+}$ (n = 1, 2, or 3) as revealed by electrochemical and UV/Vis/NIR spectral data. DFT computational studies have demonstrated that the electronic properties of the dimers reflect the extent of cluster–cluster interaction through asymmetrical bis(tridentate) triazine ligand.

Experimental Section

Materials: All manipulations were performed under dry argon using Schlenk techniques. Solvents were dried by standard methods and distilled prior to use except for spectroscopic grade solvents used for spectroscopic measurements. 3-(2-Pyridyl)-1,2,4-triazine (pytz), 3-(2-pyrimidinyl)-1,2,4-triazine (pmtz),[31] and 5,5′,6,6′-tetramethyl-3,3′-bi-1,2,4-triazine (bdmt)[32] were prepared according to literature methods. $[Ru_3O(OAc)_6(py)_2(CH_3OH)](PF_6)$ ($[\mathbf{1}]PF_6$) was synthesized according to a literature procedure.[11] Other chemicals were commercially available and used as received.

Physical Measurements: Elemental analyses were carried out with a Perkin–Elmer model 240C automatic instrument. Electrospray mass spectra (ES-MS) were recorded with a Finnigan DECAX-30000 LCQ mass spectrometer using dichloromethane/methanol as the mobile phase. The UV/Vis/NIR absorption spectra were recorded on a Perkin–Elmer Lambda 900 UV/Vis/NIR spectrometer. ^{1}H NMR spectra were recorded with a Bruker Avance III-400 spectrometer with $SiMe_4$ as the internal reference. The cyclic (CVs) and differential pulse voltammograms (DPVs) were recorded with a Potentiostat/Galvanostat Model 263A in acetonitrile solutions containing 0.1 M $(Bu_4N)PF_6$ as the supporting electrolyte. The CVs were recorded at a scan rate of 100 mV s^{-1} and the DPVs at a rate of 20 mV s^{-1} with a pulse height of 40 mV. Platinum and glassy graphite were used as counter and working electrodes, respectively, and the potentials were measured against an Ag/AgCl reference electrode. The potentials measured were always referenced to the half-wave potentials of the ferrocenium/ferrocene ($E_{½}$ = 0) couple.

Crystal Structural Determinations: Crystals of $[\mathbf{2}]PF_6{\cdot}CH_2Cl_2$, $[\mathbf{3}]PF_6{\cdot}3CH_2Cl_2$, and $[\mathbf{4}]PF_6{\cdot}½CH_2Cl_2{\cdot}H_2O$ suitable for X-ray diffraction studies were obtained by layering *n*-hexane onto their dichloromethane solutions. Single crystals sealed in capillaries with mother liquor were measured with a Rigaku SATURN70 diffractometer by using the ω scan technique with graphite-monochromated Mo-K_α radiation (λ = 0.71073 Å). The CrystalClear software package was used for data reduction and empirical absorption correction. The structures were solved by direct methods and the heavy atoms were located on an E-map. The remaining non-hydrogen atoms were determined from successive difference Fourier syntheses. All non-hydrogen atoms were refined anisotropically and the hydrogen atoms were generated geometrically and refined with isotropic thermal parameters. The structures were refined on F^2 by full-matrix least-squares methods using the SHELXTL-9[33] program package.[33]

CCDC-751866 (for **2**), -751867 (for **3**), and -751868 (for **4**) contain the supplementary crystallographic data for this paper. These data can be obtained free of charge from The Cambridge Crystallographic Data Centre via www.ccdc.cam.ac.uk/data_request/cif.

DFT Computational Methodology: All the calculations were carried out using the Gaussian 03 program package.[30] The geometrical structures of the electronic ground states and the lowest-lying triplet excited states were optimized by density functional theory (DFT)[34] with Becke's LYP (B3LYP) exchange-correlation functional.[35] There were no symmetry constraints on oxo-centered triruthenium cluster complexes **2**, **4**, $[\mathbf{5a}]^+$, and $[\mathbf{5}]^{2+}$. Based on these structures, 60 singlet states and 6 lowest triplet states were obtained to determine the vertical excitation energies for **2**, **4**, $[\mathbf{5a}]^+$, and $[\mathbf{5}]^{2+}$ in CH_2Cl_2 solution by time-dependent DFT (TD-DFT) calculations.[36,37] Solvent effects were taken into account by using the polarizable continuum model (PCM)[38] with CH_2Cl_2 as solvent. In these calculations, the Hay–Wadt double-ξ with a Los Alamos relativistic effect basis set (LANL2DZ)[39] consisting of the effective core potentials (ECP) was employed for the Ru atoms and the 6-31G (d) basis set was used for the remaining atoms. The optimized structure parameters of $[\mathbf{2}]^+$ and $[\mathbf{4}]^+$ shown in Table S2 (see Supporting Information) are in agreement with experimental values (Table 1), which indicates the accuracy of the present computational method. Calculations with significantly larger basis sets (up to 6-31+G**) were also undertaken for $[\mathbf{2}]^+$, but they did not lead to significantly different results. The charge populations and chemical bonding properties were determined by a Mulliken population analysis, which was performed by using the GGA-PW91 functional[40] of the CASTEP code[41] based on the geometry structures optimized by Gaussian 03.

$[Ru_3O(OAc)_5(py)_2\{\mu\text{-}\eta^1(N),\eta^2(N,N)\text{-pytz}\}](PF_6)$ {[2](PF$_6$)}: A dichloromethane (10 mL) solution of $[\mathbf{1}]PF_6$ (101.0 mg, 0.10 mmol) was added to a dichloromethane (15 mL) solution of pytz (19.0 mg, 0.12 mmol). The solution was stirred at room temperature for 2 days with the color changing slowly from blue to brown. The product was purified by alumina column chromatography. The second brown band was collected using dichloromethane/methanol (100:1, v/v) as eluent. The solution was reduced to a minimum volume to precipitate the product by diffusion of *n*-hexane; yield 71% (76 mg). ^{1}H NMR (CD_3CN): δ = 1.54 (s, 3 H, acetate CH_3), 1.95 (s, 3 H, acetate CH_3), 2.08 (s, 3 H, acetate CH_3), 2.15 (s, 3 H, acetate CH_3), 2.39 (s, 3 H, acetate CH_3), 7.84 (t, J = 1.76 Hz, 1 H, pyridine 5-H), 7.85 (t, J = 7.06 Hz, 2 H, pyridine *m*-H), 8.06 (d, J = 3.80 Hz, 1 H, pyridine 3-H), 8.09 (m, 1 H, pyridine 6-H), 8.15 (td, J = 6.44, 1.20 Hz, 2 H, pyridine *m*′-H), 8.24 (tt, J = 7.62, 1.47 Hz, 1 H, pyridine *p*-H), 8.36 (tt, J = 7.62, 1.54 Hz, 1 H, pyridine *p*′-H), 8.44 (td, J = 7.83, 1.42 Hz, 1 H, pyridine 4-H), 8.71 (d, J = 7.92 Hz, 1 H, triazine 5-H), 9.05 (d, J = 5.16 Hz, 2 H, pyridine *o*-H), 9.19 (dd, J = 6.36, 1.44 Hz, 2 H, pyridine *o*′-H), 9.35 (d, J = 5.16 Hz, 1 H, triazine 6-H) ppm. MS (ES): *m*/*z* (%) = 932.5 (100) $[M - PF_6]^+$. $C_{28}H_{31}F_6N_6O_{11}PRu_3{\cdot}C_6H_{14}$: calcd. C 35.15, H 3.90, N 7.23; found C 34.78, H 3.85, N 7.20.

$[Ru_3O(OAc)_5(py)_2\{\mu\text{-}\eta^1(N),\eta^2(N,N)\text{-bdmt}\}](PF_6)$ {[3](PF$_6$)}: This compound was prepared by the same synthetic procedure as described for $[\mathbf{2}]PF_6$ except for the use of bdmt (26 mg, 0.12 mmol) instead of pytz; yield 75% (85 mg). ^{1}H NMR (CD_3CN): δ = 1.54 (s, 3 H, acetate CH_3), 1.99 (s, 3 H, acetate CH_3), 2.01 (s, 3 H, acetate CH_3), 2.05 (s, 3 H, acetate CH_3), 2.21 (s, 3 H, triazine CH_3), 2.22 (s, 3 H, triazine CH_3), 2.47 (s, 3 H, acetate CH_3), 2.93 (s, 3 H, triazine CH_3), 2.96 (s, 3 H, triazine CH_3), 7.87 (t, J = 5.96 Hz, 2 H, pyridine *m*-H), 8.15 (t, J = 6.44 Hz, 2 H, pyridine *m*′-H), 8.28 (t, J = 7.60 Hz, 1 H, pyridine *p*-H), 8.35 (t, J = 7.60 Hz, 1 H, pyridine *p*′-H), 9.25 (d, J = 4.92 Hz, 4 H, pyridine *o*,*o*′-H) ppm. MS (ES): *m*/*z* (%) = 990.9 (100) $[M - PF_6]^+$. $C_{30}H_{37}F_6N_8O_{11}PRu_3{\cdot}2CH_3OH$: calcd. C 32.08, H 3.79, N 9.35; found C 32.20, H 3.71, N 9.27.

$[Ru_3O(OAc)_5(py)_2\{\mu\text{-}\eta^1(N),\eta^2(N,N)\text{-pmtz}\}](PF_6)$ {[4](PF$_6$)}: This compound was prepared by the same synthetic procedure as that described for $[\mathbf{2}]PF_6$ except for the use of pmtz (19 mg, 0.12 mmol) instead of pytz. The product was purified by alumina column

chromatography using dichloromethane/acetonitrile (10:1, v/v) as eluent; yield 78% (84 mg). ^{1}H NMR (CD_3CN): δ = 1.56 (s, 3 H, acetate CH_3), 1.96 (s, 3 H, acetate CH_3), 2.08 (s, 3 H, acetate CH_3), 2.14 (s, 3 H, acetate CH_3), 2.42 (s, 3 H, acetate CH_3), 7.84 (d, J = 3.76 Hz, 1 H, pyrimidine 5-H), 7.89 (dd, J = 7.44, 6.64 Hz, 2 H, pyridine *m*-H), 8.05 (t, J = 5.18 Hz, 1 H, pyridine *p*-H), 8.16 (m, 2 H, pyridine *m′*-H), 8.17 (m, 1 H, pyrimidine 4-H), 8.27 (t, J = 7.64 Hz, 1 H, pyrimidine 6-H), 8.36 (t, J = 7.60 Hz, 1 H, pyridine *p′*-H), 9.06 (d, J = 5.24 Hz, 2 H, pyridine *o*-H), 9.19 (d, J = 5.01 Hz, 2 H, pyridine *o′*-H), 9.42 (dd, J = 4.74, 2.10 Hz, 1 H, triazine 5-H), 9.60 (dd, J = 5.56, 2.08 Hz, 1 H, triazine 6-H) ppm. MS (ES): *m*/*z* (%) = 934.6 (100) $[M - PF_6]^+$. $C_{27}H_{30}F_6N_7O_{11}PRu_3{\cdot}CH_3CN$: calcd. C 31.16, H 2.98, N 10.02; found C 31.13, H 3.06, N 10.15.

[{Ru$_3$O(OAc)$_5$(py)$_2$}$_2${μ$_4$-η^1(C),η^1(N),η^2(N,N),η^2(N,N)-pmtz}](PF$_6$)$_2$ {[5](PF$_6$)$_2$}: A dichloromethane (15 mL) solution of [**1**]PF_6 (121.0 mg, 0.12 mmol) was added to a dichloromethane (25 mL) solution of [**4**]PF_6 (107.6 mg, 0.10 mmol) with stirring at room temperature for 2 d. The product was purified by alumina column chromatography. The third purple band was collected using dichloromethane/methanol (100:1, v/v) as eluent. The solution was reduced to a minimum volume to precipitate the product by diffusion of diethyl ether; yield 40% (79.7 mg). ^{1}H NMR (CD_3CN): δ = 1.53 (s, 3 H, acetate CH_3), 1.96 (s, 3 H, acetate CH_3), 2.00 (s, 3 H, acetate CH_3), 2.17 (s, 3 H, acetate CH_3), 4.31 (s, 6 H, acetate CH_3), 4.43 (s, 6 H, acetate CH_3), 4.52 (s, 6 H, acetate CH_3), 4.91 (m, 2 H, pyridine *m′′*-H), 4.99 (s, 1 H, pyrimidine 5-H), 5.79 (m, 1 H, pyridine *p′′*-H), 5.85 (m, 4 H, pyridine *o′′*,*o′′′*-H), 6.59 (t, J = 7.62 Hz, 2 H, pyridine *m′′′*-H), 7.63 (t, J = 5.44 Hz, 1 H, pyridine *p′′′*-H), 7.81 (t, J = 6.56 Hz, 2 H, pyridine *m*-H), 7.95 (s, 1 H, pyrimidine 6-H), 8.02 (m, 2 H, pyridine *m′*-H), 8.16 (t, J = 7.52 Hz, 1 H, pyridine *p*-H), 8.27 (m, 1 H, pyridine *p′*-H), 8.80 (d, J = 4.44 Hz, 2 H, pyridine *o*-H), 8.98 (dd, J = 4.84, 2.16 Hz, 1 H, triazine 5-H) 9.20 (d, J = 4.84 Hz, 2 H, pyridine *o′*-H), 9.38 (dd, J = 5.56, 2.16 Hz, 1 H, triazine 6-H) ppm. MS (ES): *m*/*z* (%) = 852 (100) $[M - 2PF_6]^{2+}$. $C_{47}H_{54}F_{12}N_9O_{22}P_2Ru_6{\cdot}2CH_3OH$: calcd. C 28.61, H 3.04, N 6.13; found C 28.76, H 3.13, N 5.91.

[{Ru$_3$O(OAc)$_5$(py)$_2$}$_2${μ$_4$-η^1(C),η^1(N),η^2(N,N),η^2(N,N)-pmtz}](PF$_6$) {[5a](PF$_6$)}: An excess of a 50% aqueous solution of hydrazine was added dropwise to a dichloromethane (15 mL) solution of [**5**]-$(PF_6)_2$ (100.0 mg, 0.05 mmol) with stirring until the color turned green. After stirring for 30 min, distilled water (25 mL) was added to the solution. The stirring was continued for a further 10 min and then the dichloromethane layer was separated in an extraction funnel. The product was crystallized twice by layering *n*-hexane onto the dichloromethane solution and dried in vacuo; yield 75% (70 mg). MS (ES): *m*/*z* (%) = 1704 (100) $[M - PF_6]^+$. $C_{47}H_{54}F_6N_9O_{22}PRu_6{\cdot}^3/_2C_6H_{14}$: calcd. C 34.01, H 3.82, N 6.37; found C 34.26, H 4.10, N 6.63.

[{Ru$_3$O(OAc)$_5$(py)$_2$}$_2${μ$_4$-η^1(C),η^1(N),η^2(N,N),η^2(N,N)-pmtz}](PF$_6$)$_3$ {[5b](PF$_6$)$_3$}: A dichloromethane (5 mL) solution of ferrocenium hexafluorophosphate (16.6 mg, 0.05 mmol) was added dropwise to a dichloromethane (10 mL) solution of [**5**]$(PF_6)_2$ (100.0 mg, 0.05 mmol). The color changed from purple to blue on stirring for 30 min. The solution was concentrated to around 3 mL and then *n*-hexane was added to precipitate the product. It was recrystallized twice in acetonitrile/diethyl ether to give the product; yield 72% (77 mg). MS (ES): *m*/*z* (%) = 568.3 (100) $[M - 3PF_6]^{3+}$. $C_{47}H_{54}F_{18}N_9O_{22}P_3Ru_6{\cdot}2Et_2O{\cdot}2CH_3CN$: calcd. C 29.92, H 3.40, N 6.50; found C 29.96, H 3.34, N 6.42.

Supporting Information (see footnote on the first page of this article): ES–MS, ^{1}H NMR and UV/Vis spectra, CVs and DPVs, and the results of DFT calculation.

Acknowledgments

This work was financially supported by the National Natural Science Foundation of China (NSFC) (grant numbers 20821061, 20931006, and U0934003), the 973 project from the Ministry of Science and Technology of China (MSTC) (grant 2007CB815304), and the National Science Foundation (NSF) of Fujian Province (grant 2008I0027).

[1] S. J. Lippard, *Angew. Chem. Int. Ed. Engl.* **1988**, *27*, 344–361.
[2] C. Wilson, B. B. Iversen, J. Overgaard, F. K. Larsen, G. Wu, S. P. Palii, G. A. Timco, N. V. Gerbeleu, *J. Am. Chem. Soc.* **2000**, *122*, 11370–11379.
[3] a) A. L. Feig, S. J. Lippard, *Chem. Rev.* **1994**, *94*, 759–805; b) E. L. Solomon, T. C. Brunold, M. I. Davis, J. N. Kemsley, S. K. Lee, N. Lehnert, F. Neese, A. J. Skulan, Y. S. Yang, J. Zhou, *Chem. Rev.* **2000**, *100*, 235–350.
[4] a) S. Saito, Y. Yamamoto, *Chem. Rev.* **2000**, *100*, 2901–2916; b) T. Y. Luh, M. K. Leung, K. T. Wong, *Chem. Rev.* **2000**, *100*, 3187–3204; c) R. Breslow, S. D. Dong, *Chem. Rev.* **1998**, *98*, 1997–2012.
[5] a) M. Fujita, Y. J. Kwon, S. Washizu, K. Ogura, *J. Am. Chem. Soc.* **1994**, *116*, 1151–1152; b) L. Chen, H. Yu, L. Wu, W. X. Du, X. C. Gao, P. Lin, W. J. Zhang, C. P. Cui, X. T. Wu, *J. Solid State Chem.* **2000**, *151*, 286–293.
[6] a) K. D. Demadis, C. M. Hartshorn, T. J. Meyer, *Chem. Rev.* **2001**, *101*, 2655–2686; b) F. Paul, C. Lapinte, *Coord. Chem. Rev.* **1998**, *178–180*, 431–509.
[7] a) F. A. Cotton, C. Lin, C. A. Murillo, *Acc. Chem. Res.* **2001**, *34*, 759–771; b) F. Barigelletti, L. Flamigni, *Chem. Soc. Rev.* **2000**, *29*, 1–12; c) D. Astruc, *Acc. Chem. Res.* **1997**, *30*, 383–391; d) W. Kaim, A. Klein, M. Glöckle, *Acc. Chem. Res.* **2000**, *33*, 755–763.
[8] a) R. L. Carroll, C. B. Gorman, *Angew. Chem. Int. Ed.* **2002**, *41*, 4378–4400; b) Y. Hoshino, S. Higuchi, J. Fiedler, C.-Y. Su, A. Knödler, B. Schwederski, B. Sarkar, H. Hartmann, W. Kaim, *Angew. Chem. Int. Ed.* **2003**, *42*, 674–677; c) C. Patoux, J.-P. Launay, M. Beley, S. Chodorowski-Kimmes, J.-P. Collin, S. James, J.-P. Sauvage, *J. Am. Chem. Soc.* **1998**, *120*, 3717–3725.
[9] a) R. H. Laye, S. M. Couchman, M. D. Ward, *Inorg. Chem.* **2001**, *40*, 4089–4092; b) P. J. Mosher, G. P. A. Yap, R. J. Crutchley, *Inorg. Chem.* **2001**, *40*, 1189–1195; c) C. C. Cameron, P. G. Pickup, *J. Am. Chem. Soc.* **1999**, *121*, 7710–7711.
[10] a) A. Spencer, G. Wilkinson, *J. Chem. Soc., Dalton Trans.* **1972**, 1570–1577; A. Spencer, G. Wilkinson, *J. Chem. Soc., Dalton Trans.* **1974**, 786–792.
[11] J. A. Baumann, D. J. Salmon, S. T. Wilson, T. J. Meyer, W. E. Hatfield, *Inorg. Chem.* **1978**, *17*, 3342–3350.
[12] a) H. Kido, H. Nagino, T. Ito, *Chem. Lett.* **1996**, 745–746; b) D. Akashi, H. Kido, M. Abe, Y. Sasaki, T. Ito, *Dalton Trans.* **2004**, 2883–2889; c) Y. Zhang, Y. Tong, M. Abe, K. Uosaki, M. Osawa, Y. Sasaki, S. Ye, *J. Mater. Chem.* **2009**, *19*, 261–267; d) H. Uehara, T. Inomata, M. Abe, K. Uosaki, Y. Sasaki, *Chem. Lett.* **2008**, *37*, 684–685; e) M. Abe, T. Masuda, T. Kondo, K. Uosaki, Y. Sasaki, *Angew. Chem. Int. Ed.* **2005**, *44*, 416–419; f) T. Michi, M. Abe, J. Matsuno, K. Uosaki, Y. Sasaki, *Bull. Chem. Soc. Jpn.* **2007**, *80*, 1368–1386.
[13] H. E. Toma, K. Araki, A. D. P. Alexiou, S. Nikolaou, S. Dovidauskas, *Coord. Chem. Rev.* **2001**, *219–221*, 187–234.
[14] Z.-N. Chen, F. R. Dai, *Struct. Bonding (Berlin)* **2009**, *133*, 93–120.
[15] a) S. T. Wilson, R. F. Bondurant, T. J. Meyer, D. J. Salmon, *J. Am. Chem. Soc.* **1975**, *97*, 2285–2287; b) J. A. Baumann, S. T. Wilson, D. J. Salmon, P. L. Hood, T. J. Meyer, *J. Am. Chem. Soc.* **1979**, *101*, 2916–2920; c) J. A. Baumann, D. J. Salmon, S. T. Wilson, T. J. Meyer, *Inorg. Chem.* **1979**, *18*, 2472–2479.
[16] a) M. Abe, Y. Sasaki, Y. Yamada, K. Tsukahara, S. Yano, T. Yamaguchi, M. Tominaga, I. Taniguchi, T. Ito, *Inorg. Chem.*

1996, *35*, 6724–6734; b) M. Abe, Y. Sasaki, Y. Yamada, K. Tsukahara, S. Yano, T. Ito, *Inorg. Chem.* **1995**, *34*, 4490–4498.
[17] a) S. A. Fouda, G. L. Rempel, *Inorg. Chem.* **1979**, *18*, 1–8; b) C. Bilgrien, S. Davis, R. S. Drago, *J. Am. Chem. Soc.* **1987**, *109*, 3786–3787.
[18] a) L. Vieille-Petit, G. Süss-Fink, B. Therrien, T. R. Ward, H. Stoeckli-Evans, G. Labat, L. Karmazin-Brelot, A. Neels, T. Bürgi, R. G. Finke, C. M. Hagen, *Organometallics* **2005**, *24*, 6104–6119; b) M. Itou, M. Otake, Y. Araki, O. Ito, H. Kido, *Inorg. Chem.* **2005**, *44*, 1580–1587.
[19] F.-R. Dai, B. Li, L.-X. Shi, L.-Y. Zhang, Z.-N. Chen, *Dalton Trans.* **2009**, 10244–10249.
[20] S. Nikolaou, H. E. Toma, *Eur. J. Inorg. Chem.* **2008**, 2266–2271.
[21] G. S. Nunes, A. D. P. Alexiou, H. E. Toma, *J. Catal.* **2008**, *260*, 188–192.
[22] K. Ota, H. Sasaki, T. Matsui, T. Hamaguchi, T. Yamaguchi, T. Ito, H. Kido, C. P. Kubiak, *Inorg. Chem.* **1999**, *38*, 4070–4078.
[23] a) M. Abe, Y. Sasaki, T. Yamaguchi, T. Ito, *Bull. Chem. Soc. Jpn.* **1992**, *65*, 1585–1590; b) M. Abe, A. Sato, T. Inomata, T. Kondo, K. Uosaki, Y. Sasaki, *J. Chem. Soc., Dalton Trans.* **2000**, 2693–2702; c) Y. Sasaki, A. Tokiwa, T. Ito, *J. Am. Chem. Soc.* **1987**, *109*, 6341–6347.
[24] a) S. H. Toma, S. Nikolaou, D. M. Tomazela, M. N. Eberlin, H. E. Toma, *Inorg. Chim. Acta* **2004**, *357*, 2253–2260; b) S. Nikolaou, H. E. Toma, *J. Chem. Soc., Dalton Trans.* **2002**, 352–359; c) S. Ye, W. Zhou, M. Abe, T. Nishida, L. Cui, K. Uosaki, M. Osawa, Y. Sasaki, *J. Am. Chem. Soc.* **2004**, *126*, 7434–7435.
[25] a) J. L. Chen, X. D. Zhang, L. Y. Zhang, L. X. Shi, Z. N. Chen, *Inorg. Chem.* **2005**, *44*, 1037–1043; b) F.-R. Dai, J.-L. Chen, H.-Y. Ye, L.-Y. Zhang, Z.-N. Chen, *Dalton Trans.* **2008**, 1492–1502; c) H. Yuge, S.-i. Asahi, T. K. Miyamoto, *Dalton Trans.* **2009**, 2287–2289.
[26] H.-Y. Ye, L.-Y. Zhang, J.-L. Chen, Z.-N. Chen, *Chem. Commun.* **2006**, 1971–1973.
[27] a) H.-Y. Ye, F.-R. Dai, L.-Y. Zhang, Z.-N. Chen, *Inorg. Chem.* **2007**, *46*, 6129–6135; b) F.-R. Dai, H.-Y. Ye, B. Li, L.-Y. Zhang, Z.-N. Chen, *Dalton Trans.* **2009**, 8696–8703.
[28] F. A. Cotton, J. G. Norman Jr., *Inorg. Chim. Acta* **1972**, *6*, 411–419.
[29] T. Hamaguchi, H. Nagino, K. Hoki, H. Kido, T. Yamaguchi, B. K. Breedlove, T. Ito, *Bull. Chem. Soc. Jpn.* **2005**, *78*, 591–598.
[30] M. J. Frisch, G. W. Trucks, H. B. Schlegel, G. E. Scuseria, M. A. Robb, J. R. Cheeseman, J. A. Montgomery Jr., T. Vreven, K. N. Kudin, J. C. Burant, J. M. Millam, S. S. Iyengar, J. Tomasi, V. Barone, B. Mennucci, M. Cossi, G. Scalmani, N. Rega, G. A. Petersson, H. Nakatsuji, M. Hada, M. Ehara, K. Toyota, R. Fukuda, J. Hasegawa, M. Ishida, T. Nakajima, Y. Honda, O. Kitao, H. Nakai, M. Klene, X. Li, J. E. Knox, H. P. Hratchian, J. B. Cross, V. Bakken, C. Adamo, J. Jaramillo, R. Gomperts, R. E. Stratmann, O. Yazyev, A. J. Austin, R. Cammi, C. Pomelli, J. W. Ochterski, P. Y. Ayala, K. Morokuma, G. A. Voth, P. Salvador, J. J. Dannenberg, V. G. Zakrzewski, S. Dapprich, A. D. Daniels, M. C. Strain, O. Farkas, D. K. Malick, A. D. Rabuck, K. Raghavachari, J. B. Foresman, J. V. Ortiz, Q. Cui, A. G. Baboul, S. Clifford, J. Cioslowski, B. B. Stefanov, G. Liu, A. Liashenko, P. Piskorz, I. Komaromi, R. L. Martin, D. J. Fox, T. Keith, M. A. Al-Laham, C. Y. Peng, A. Nanayakkara, M. Challacombe, P. M. W. Gill, B. Johnson, W. Chen, M. W. Wong, C. Gonzalez, J. A. Pople, *Gaussian 03*, rev. B, Gaussian Inc., Pittsburgh, PA, **2003**.
[31] T. Shintou, F. Ikeuchi, H. Kuwabara, K. Umihara, I. Itoh, *Chem. Lett.* **2005**, *34*, 836–837.
[32] J. Breu, K.-J. Range, E. Herdtweck, *Monatsh. Chem.* **1993**, *125*, 119–140.
[33] G. M. Sheldrick, *SHELXL-97, Program for the Refinement of Crystal Structures*, University of Göttingen, Germany, **1997**.
[34] A. D. Becke, *J. Chem. Phys.* **1993**, *98*, 5648.
[35] a) A. D. Becke, *Phys. Rev. A* **1988**, *38*, 3098–3100; A. D. Becke, *J. Chem. Phys.* **1992**, *96*, 2155–2160; b) C. Lee, W. Yang, R. Parr, *Phys. Rev. B* **1988**, *37*, 785–789.
[36] M. E. Casida, C. Jamorski, K. C. Casida, D. R. Salahub, *J. Chem. Phys.* **1998**, *108*, 4439.
[37] R. E. Stratmann, G. E. Scuseria, M. J. Frisch, *J. Chem. Phys.* **1998**, *109*, 8218.
[38] a) B. Mennucci, J. Tomasi, *J. Chem. Phys.* **1997**, *106*, 5151–5158; b) M. Cossi, G. Scalmani, N. Regar, V. Barone, *J. Chem. Phys.* **2002**, *117*, 43; c) V. Barone, M. J. Cossi, *Chem. Phys.* **1997**, *107*, 3210.
[39] a) W. R. Wadt, P. J. Hay, *J. Chem. Phys.* **1985**, *82*, 284; b) P. J. Hay, W. R. Wadt, *J. Chem. Phys.* **1985**, *82*, 299.
[40] J. P. Perdew, J. A. Chevary, S. H. Vosko, K. A. Jackson, M. R. Pederson, D. J. Singh, C. Fiolhais, *Phys. Rev. B* **1992**, *46*, 6671–6687.
[41] M. D. Segall, P. L. D. Lindan, M. J. Probert, C. J. Pickard, P. J. Hasnip, S. J. Clark, M. C. Payne, *J. Phys.: Condens. Matter* **2002**, *14*, 2717–2744.

Received: January 26, 2011
Published Online: April 1, 2011

